Title
CHEMISORPTION STRUCTURE OF C(2X2)S/FE(001) DETERMINED BY ARPEFS

Authors
Zhang, X.S.
Terminello, L.J.
Kim, S.

Publication Date
1988-03-01

LBL-24248
Preprint

Lawrence Berkeley Laboratory
UNIVERSITY OF CALIFORNIA

Materials & Chemical Sciences Division

Submitted to Journal of Chemical Physics

Chemisorption Structure of c(2x2)S/Fe(001) Determined by ARPEFS

X.S. Zhang, L.J. Terminello, S. Kim, Z.Q. Huang,
A.E. Schach von Wittenau, and D.A. Shirley

March 1988

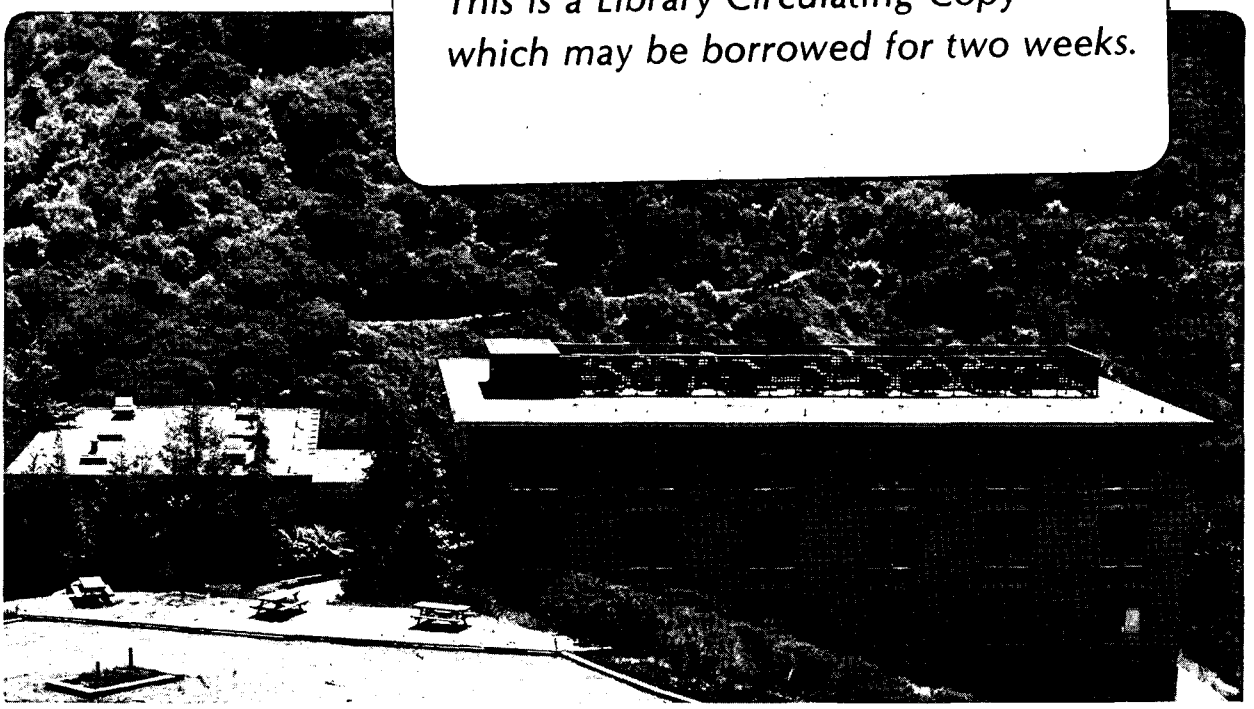

Prepared for the U.S. Department of Energy under Contract Number DE-AC03-76SF00098.

DISCLAIMER

LBL-24248

Chemisorption Structure of c(2x2)S/Fe(001) Determined by ARPEFS

X.S. Zhang,* L.J. Terminello, S. Kim,† Z.Q. Huang,
A.E. Schach von Wittenau, and D.A. Shirley

Department of Chemistry, University of California
and
Materials and Chemical Sciences Division
Lawrence Berkeley Laboratory, 1 Cyclotron Road
Berkeley, California 94720

---

*Present address: Physics Department Zhejiang University, Hangzhou, People's Republic of China.

†Present address: Korea Institute of Technology, Taejon, Choongchungnam-do 300-31, Korea.

Abstract

An accurate chemisorption geometry was determined for the c(2x2)S/Fe(001) system using the angle-resolved photoemission extended fine structure (ARPEFS) method, with S(1s) photoelectron peak intensities observed along [001] and [011]. Multiple-scattering spherical-wave analysis confirmed the LEED-derived fourfold hollow site geometry, and yielded perpendicular distances for S of 1.09(2)Å above the first layer and 2.50(2)Å above the second layer atom directly below S. The S-Fe nearest-neighbor bond length is 2.30(1)Å and the M-S-M bond angle is 123(1)°. The Fe_1-Fe_2 interlayer distance is contracted to 1.40(2)Å and the Fe_2-Fe_3 distance expanded to 1.46(3)Å, relative to the bulk value of 1.43Å. The results are compared with similar systems and partially explained on chemical grounds. The derived structure agrees with the results of a self-consistent field (SCF) Xα spherical wave (SW) calculation.

I. Introduction

The surface structures of chalcogens atomically adsorbed on transition-metal surfaces are of interest both in understanding the surface chemical bond and for their relevance to such processes as corrosion and catalyst poisoning. We have studied the system c(2x2)S/Fe(001) as part of a program which has the dual goals of establishing the systematic variation of similar structures to a high level of accuracy and of providing further insights about the photoelectron diffraction method. The related systems c(2x2)S/Cr(001)[1] and c(2x2)P/Fe(001)[2] are also under study, in hopes of using these high Debye temperature lattices to advantage in studying the local geometry around the adsorbate atoms on body-centered cubic metals.

The c(2x2)S/Fe(001) system has been studied by several groups.[3-7] In a low energy electron diffraction (LEED) study, Legg et al.[3] reported a fourfold hollow site symmetry for sulfur, with a perpendicular distance of 1.09(5)Å, with an assumed Fe_I-Fe_{II} first-to-second layer distance of 1.43Å, equal to the bulk value. Thus our specific structural goals in this research were, first, to confirm the LEED structure and, second, to improve the accuracy of the structural parameters, if possible, thereby providing a stronger data base upon which the surface bonding can ultimately be understood. These goals were achieved, as reported below.

To study the c(2x2)S/Fe(001) system we used the photoelectron diffraction method termed angle-resolved photoemission extended fine structure (ARPEFS), developed in this laboratory and described by Barton, et al.[8-10] with an EXAFS-like theoretical model. In the

application of ARPEFS to the c(2x2)S/Fe(001) system, synchrotron radiation was used to excite photoelectrons from the S(1s) orbital. Detection of S(1s)-derived photoelectrons emitted in selected directions--[001] and [011] in this case--allowed the observation of very large interference effects between the primary (unscattered) photoelectron wave originally propagating along e.g., [001] and contributions that arise through elastic scattering of the primary wave off neighboring atoms into the [001] direction. The interference depends upon kR, the phase gained by the scattered electron of wavenumber k in travelling through an additional path-length difference R. The ARPEFS method is designed to exploit the sensitivity of this interference effect to R by varying k; i.e., by "sweeping" the photoelectron energy through tuning of the exciting photon's energy $h\nu$. The extreme angular sensitivity was exploited in this structure by choosing directions that maximize backscattering off the two inequivalent second layer Fe atoms.

Experimental procedures are discussed in Section II. Data reduction and results are presented in Section III. In Section IV the structural results are discussed in the context of similar systems and theoretical models.

II. Experimental

The experiments were performed on Beam Line III-3 at the Stanford Synchrotron Radiation Laboratory, using photons in the energy range $h\nu$ = 2500-3000 eV provided by a Ge(111) double-crystal monochromator. The double crystal rocking curves showed an energy resolution increasing from 1.3 eV to 1.6 eV through this range.[11] Our S(1s) photoelectron peaks included additional broadening from lifetime and instrumental effects, resulting in total observed peak widths varying from 2.1 eV to 2.6 eV FWHM with increasing energy. The double Bragg reflection geometry significantly enhances the already high degree of linear polarization of the incident synchrotron radiation.[11] For the conditions of this experiment a polarization of 98% can be estimated.

The experimental chamber[12] had a base pressure of 1.8×10^{-10} Torr. A hemispherical angle-resolved multichannel analyzer with complete two-axis angular motion was used to collect and analyze the photoelectrons. The effective angular resolution, measured always in terms of the effective opening half angle θ_e, ranged between $\theta_e = 1.8°$ for the highest kinetic energies, close to $\theta_e = 2.0°$ over most of the range, and rising to $\theta_e = 3°$ for the lowest kinetic energies. Of the three factors that control θ_e, two are readily modelled. These are the (geometrical) half angle opening, θ_s, for electrons from a point source entering the first lens, and the half angle opening, θ_a, for electrons accepted into the analyzer. The Helmholtz-Lagrange law

$$\theta_s E_k^{1/2} = \theta_a E_p^{1/2}$$

relates these angles, the initial kinetic energy E_k and the analyzer pass energy E_p.[12] The third factor is finite source size. When convoluted into the above relation, with E_p = 160 eV, it leads to the stated range θ_e = 1.8-3.0°.

The iron crystal was cut from a 6 mm diameter boule using an electronic discharge cutter, polished, with the final polish employing 0.5 μm mesh Al_2O_3 powder, and etched. The Fe(001) surface was selected with ±1° precision by Laue backscattering. Iron is difficult to clean; the bcc-to-fcc transition at 910°C mandates a practical cleaning temperature range of 800°C and below. The sample surface was cleaned of its major contaminants--oxygen, sulfur, and carbon--by repeated sputter-anneal cycles in the UHV chamber. We used an Ar ion beam at a beam voltage of 1.0 kV and an emission current of 20 mA, and annealed at 700°C. Repeated cycles over a period of 5 weeks depleted C, S, and O from the bulk, and an ordered surface could thereafter be recovered by annealling at 550°C. Recleaning after each set of measurements required only Ar^+ sputtering at 500 V, followed by a few-minute anneal at 550°C. Temperatures were measured by a chromel alumel thermocouple near the sample, calibrated with an infrared pyrometer.

The LEED pattern of the clean surface showed a clear and sharp (1x1) structure. The bulk contaminants C, O, and S were monitored by Auger electron spectroscopy (AES) using four-grid LEED optics in the retarding field mode, and were found to be within the noise level of the measurement. The c(2x2) overlayer of sulfur was prepared by exposure to H_2S gas (Matheson, Inc.) using an effusive beam doser, followed by

annealing to 500°C. AES measurements on c(2x2)S/Fe(001) showed no detectable contaminants before and after taking the ARPEFS data.

Narayan et al.[13] indicated that H_2S dissociates when the substrate temperature reaches 190K; Shanbarger[14] has described similar results. Hydrogen desorbs after annealing to 500°C.

Photoemission spectra were taken in two geometries. The two emission angles chosen for the ARPEFS measurements were aligned with the [001] and [011] crystallographic directions. Both directions exploit ARPEFS's backscattering sensitivity in order to give detailed interlayer spacing information. Backscattering in the [001] geometry is most sensitive to the position of the second-layer Fe atoms directly below the S atoms, while [011] backscattering is sensitive to the other second-layer Fe atoms, equal in number, that lie below open sites. Taken together, the relative positions of the two inequivalent types of second-layer Fe atoms would establish the extent to which the second layer is buckled upon S adsorption.

The emission angles for the two geometries were aligned by He-Ne laser auto-collimation through a chamber viewport, with a precision[15] of ± 2° referenced to the surface of a vacuum chamber window. The [001] geometry had the photon polarization vector 35° from the surface normal toward [011], while the [011] emission direction had the polarization vector along [011]. The experimental geometries are shown in Fig. 1.

III. Data Analysis and Results

The primary ARPEFS data consisted of five sets of S(1s) photoelectron spectra, three in the [001] geometry and two in the [011] geometry. In each data set the photon energy $h\nu$ was stepped through a range of values to give S(1s) photoelectron kinetic energies spaced at equal increments of electron wavenumber, k. The increment selected was 0.10Å^{-1}, and the k values were staggered within each of the two pairs of data sets ([001] and [011]) with the best statistics, which were used in the final analysis. This staggering format provided a test of reproducibility and in the [001] emission case an estimate of the statistical variance. Photon energy and k are related by

$$h\nu = E_B^V(S1s) - V_o + \frac{\hbar^2k^2}{2m}$$

where $E_B^V(S1s)$ is the S(1s) binding energy relative to the vacuum energy, V_o is the inner potential, and $\frac{\hbar^2k^2}{2m}$ is the electron kinetic energy.

Peak intensities and the ARPEFS function $\chi(k)$ were derived as follows.[16] The electron inelastic scattering background intensity, to which our peak intensities were normalized was established as a universal function over the kinetic energy range 50-600 eV from electron emission spectra taken with photon energies of 2500 eV and 2700 eV. The photoelectron peak (and tail) response function itself includes the effects of lifetime broadening (Lorentzian) and inelastic scattering (a Gaussian convoluted with a step function) as well as instrumental broadening effects (Gaussian). The S(1s) photopeaks were modelled by a combination of these functions and the inelastic background derived

from the universal curves. The photoemission intensity was normalized to this background on the high kinetic energy side of the S(1s) peak. Since this inelastic background is derived from scattered substrate photoelectrons and Auger electrons, it should provide a very reliable measure of the appropriate normalization factor for the ARPEFS experiment, including the effects of instrumental geometry and efficiency. Experience[16] with other systems has confirmed this expectation.

The S(1s)-induced intensity was isolated and normalized, by fitting a Voigt function for the peak and a Gaussian step function for the S(1s)-induced inelastic "tail" at lower kinetic energies. Only the Voigt peak area was used for $\chi(E)$. The Voigt function is a convolution of a Gaussian and a Lorentzian with a common mean. Most instrumental broadening effects have Gaussian profiles, and the Lorentzian contribution should be S(1s)-lifetime derived and independent of the photoelectron energy. In fact, the Lorentzian width was optimized at a constant value of 0.8 eV throughout the data set, in reasonable agreement with the estimated natural linewidth of 0.6 eV for atomic sulfur.[1]

In analogy with the conventional treatment of EXAFS data, the energy dependent peak intensities I(E) derived as illustrated above can be described as arising through modulation of an intrinsic photopeak intensity $I_o(E)$ by an oscillatory scattering function $\chi(E)$:

$$I(E) = [1 + \chi(E)]\ I_o(E). \qquad (1)$$

Here $I_o(E)$ is closely related to the S(1s) cross-section $\sigma(E)$, but we do not feel confident that we could model $I_o(E)$ accurately with a theoretical $\sigma(E)$ curve. Instead we prefer to simulate $I_o(E)$ with a low-order polynomial[15] or a cubic spline fit, as in EXAFS.[17] Because $I_o(E)$ is a slowly-varying function this procedure introduces negligible errors, for the range of $I_o(E)$ functions that we might use.[16] Following this fit we then solved for

$$\chi(E) = I(E)/I_o(E) - 1. \qquad (2)$$

Prior to further analysis, it was convenient to convert $\chi(E)$ to $\chi(k)$, using the relation $k = 0.512\ (E+V_o)^{1/2}\ \text{Å}^{-1}$, with E and V_o expressed in eV units. The inner potential V_o is, in a "nearly-free-electron" model, related to the bottom of the valence bands, 10-15 eV below the vacuum level, E^V. In the ARPEFS analysis V_o is treated as an adjustable parameter, similar to both EXAFS and LEED. We found V_o = 14.5 eV by an iterative process. We note that this V_o value should not be compared with LEED-derived V_o's. In LEED V_o is often taken as a complex potential, and adjusted to account for some inelastic processes. Because of this and/or the lower kinetic energies, there appears to be a higher sensitivity[18] of derived structural parameters to V_o in LEED than in ARPEFS. Figure 2 shows the $\chi(k)$ curves derived from the [001] and [011] data.

The analysis of ARPEFS $\chi(k)$ data yields scattering path-length differences

$$\Delta R_j = r_j(1 - \cos \theta_j) \qquad (3)$$

which would appear, for example, in simple single-scattering ARPEFS theory as[16]

$$\chi(k) = \sum_j A_j(k)\cos(k\Delta R_j + \phi_j). \qquad (4)$$

Here $A_j(k)$ contains thermal, inelastic scattering, etc. factors, r_j is the bond length, θ_j the scattering angle, ϕ_j the scattering phase shift, and j indexes the scattering atoms.

ARPEFS data analysis essentially yields a set of ΔR_j values, hence a chemisorption geometry. It is prudent, although not necessary, to first Fourier analyze $\chi(k)$, obtaining semi-quantitative ΔR_j values and a rough local site geometry. Next we fit $\chi(k)$ itself, using Multiple-Scattering Spherical Wave (MSSW) theory,[10] to extract accurate structural parameters. These two steps are discussed separately below.

A. Fourier Analysis.

Fourier analysis of the ARPEFS $\chi(k)$ data yields peaks near ΔR_j values which depend strongly on the experimental geometry. In particular the Fourier spectrum varies strongly both with the local site geometry--bond directions and angles--and with emission angle. Thus Fourier transforms of data from two or more emission directions, such as [001] and [011], yield a direct and absolute surface structure determination. Figure 3 shows Fourier transforms of the [001] and [011] $\chi(k)$ data for c(2x2)S/Fe(001).

The Fourier spectra are clearly very distinctive, with several clearly discernible peaks in both the [001] and [011] spectra. The difference between the two is equally remarkable, as it demonstrates the directional sensitivity of ARPEFS. More important, it allows very accurate directional information to be derived. We proceed now to establish the adsorbate system geometry by inspection of Fig. 3, with reference to Fig. 4, in which the atoms that make the largest contributions to each of several peaks in the Fourier spectra are given the same labels as the peaks in Fig. 3.

We start with the well-known result that forward (scattering angle θ=0°) and back (θ=180°) scattering tend to be strongest over this range of k. From simple geometry it follows that, with the source atom in an adsorbate overlayer, intense peaks with the smallest ΔR_j values will require large scattering angle events except for electron propagation directions relatively close to the surface (e.g., as in azimuthal photoelectron diffraction). Thus backscattering through θ_j = 180° should be especially strong in ARPEFS spectra, and from Eq. 3, a strong peak at $\Delta R_j \sim 2r_j$ is expected if a near-neighbor substrate atom lies at a distance r_j directly behind the source atom. For S-Fe scattering, the sum of covalent radii gives $r_j \sim 2.48$Å: thus a peak at $R_j \sim 4.96$Å could arise through backscattering from a "touching" nearest neighbor. The peak at $\Delta R_j \sim 4.80$Å in the [001] Fourier spectrum of Fig. 3 would be a candidate for backscattering off a first-layer Fe atom, with S in the "atop" geometry. This is clearly not correct, however, because in the "atop" geometry, there would be no scatterers with ΔR_j values small enough to produce either the large peak at 3.84Å labelled "1" in the

[011] spectrum or the partially resolved feature labelled "1" near 3Å in the [001] spectrum.

A similar process eliminates a "bridge" bonding geometry as a possibility. The absence of a strong backscatterer in the bridge site leaves the peak at 4.8Å in the [001] spectrum unexplained. By further arguments all but the fourfold hollow geometry can be eliminated.

With a trial fourfold hollow site geometry the main Fourier spectral features fall nicely into place. With the S atom 1.1Å above the first-layer Fe atoms, the peak at 4.8Å in the [001] spectrum is dominated by strong $\theta = 180°$ backscattering off the second-layer Fe atom directly below (labelled "2") which as we shall show later, has an Fe-S scattering path-length distance only slightly larger than the first-layer nearest neighbors. This is possible because of the relatively open bcc (001) face. The smaller peak at ~ 3.3Å arises largely from the four nearest neighbors (geometry alone would give $\Delta R \sim 3.4$Å), labelled "1", which scatter weakly at $\theta = 119°$, and a stronger peak near 8.3Å attributed mainly to the four third-layer atoms (Geometric $\Delta R = 8.15$Å) labelled "3" scattering through $\theta = 153°$. Peak 4 is derived in part through backscattering off the fourth-layer Fe atom directly below the S atom.

Similar relations exist between the peaks in Fig. 3 and the labelled atoms in Fig. 4, for the [011] spectrum. We believe that the fourfold hollow adsorption-site geometry is unambiguously established from the Fourier spectra. However, we have been careful not to attribute any peak entirely to a single type of scatterer. There are in

fact many scatterers with $\Delta R_j < 10$Å whose contributions are too large to ignore. This complexity precludes deriving accurate distances through backtransforming the Fourier peaks, for example. We close our discussion of the Fourier transform analysis by noting that the major [001] peaks are spaced more closely than are the [011] peaks. This difference corresponds, both in ratio and in magnitude (2.86Å vs. 4.04Å) to the interplanar spacing in the two directions, and we believe it is due to the dominance of backscattering. While the case would not be convincing based on these spectra alone, we have now observed the effect in ARPEFS data on several systems.

B. Multiple Scattering Analysis.

While a single-scattering plane-wave model can give $\chi(k)$ curves that simulate the experimental data fairly well, Barton et al.[10] showed that a really quantitative interpretation of ARPEFS data requires both multiple scattering and spherical waves. They developed a Taylor series magnetic quantum number expansion (TS-MQNE) approximation for generating multiple-scattering spherical-wave (MSSW) curves. This approach permits economic MSSW calculations that include important physical aspects of the problem.

Let us first consider the "non-structural" parameters in the calculations. The sulfur and iron phase shifts were calculated using a modified version of a program developed by Pendry.[19] The iron potential came from the self-consistent local density approximation (LDA) calculations of Moruzzi et al.[20] Sulfur phase shifts were calculated by Robey at al.,[21] using a potential obtained from Hartree-Fock wave

functions. A total of 17 calculated partial wave phase shifts were used for our simulations. Inelastic damping was taken to vary as $e^{-r/\lambda}$, and the mean free path λ was taken as 0.753k, similar to the value used in the Ni ARPEFS work.[10] The surface Debye temperature is expected to be different from that of the bulk. The bulk Debye temperature of iron was taken as θ_D(Fe, bulk) = 420K, and for the surface Θ_D(Fe, surface) = 297K, following procedures used in EXAFS[15] adapted for ARPEFS.[10] Finally, for sulfur on iron, the mean-square oscillations were estimated, following the work of Allen, et al.,[22] who related the mean-square displacement and mass by $\langle u_i^2 \rangle M_i^{1/2}$ = constant. The final effective surface Debye temperature for the surface sulfur is θ_D(S, surface) = 395K.

With the non-structural parameters selected, we proceeded to derive structural information by fitting the χ(k) data using MSSW theory. First, three unreconstructed test geometries--atop, bridge, and fourfold hollow--were computed, with the nearest-neighbor Fe-S bond length taken as 2.30Å, consistent with the LEED value[3] and close to estimates based on covalent radii. The results, shown in Figs. 5 and 6, confirm the fourfold hollow site geometry and eliminate the other two, consistent with the Fourier transform analysis. This also agrees with the LEED result.[3]

With the adsorption site geometry established, the structural factors were then optimized to find an absolute minimum in an r-factor, defined[21] as

$$r = \frac{\int[\chi_e(k)-\chi_t(k)]^2 dk}{\int[\chi_e(k)]^2 dk}$$

where $\chi_e(k)$ and $\chi_t(k)$ denote, respectively, the wavevector dependent experimental and theoretical ARPEFS $\chi(k)$.

After the first optimization between these two parameters yielded S-Fe_1 = 1.09Å, S-Fe_2 = 2.50Å, additional parameters were varied and the fits were re-optimized, all without affecting the resulting parameters materially. For example the exact emission directions were optimized to better precision than they could be measured under experimental conditions. Other (deeper) interlayer spacings were varied, and we also tested for corrugation of the second layer.[23] Calculations with a high density of parameter space points yielded final values for S-Fe_1, S-Fe_2, and S-Fe_3 as listed in Table I, with no second-layer corrugation (to within 0.03Å) or variations from bulk-value positions for other atoms. Fig. 7 shows the best MSSW fits to $\chi(k)$ for both data sets.

IV. Discussion.

The development of ARPEFS and other high-accuracy methods for determining surface structures, together with systematic studies of series of related structures, should help to advance our understanding of the surface chemical bond. We should, for example, be able to go beyond simply noting that a given structure is fourfold hollow, and develop some understanding of why structural parameters have certain values in terms of arguments based on chemical bonding and steric factors. We shall present such arguments for c(2x2)S/Fe(001) below.

First, however, let us discuss errors, to develop a sense of how far a discussion of structural parameters can meaningfully be taken.

The errors in our results arise from several sources. The "physical" errors such as crystal alignment and variation in the photon intensity during normalization background measurement, as well as statistical errors and errors in extracting peak intensities from data, are very small, especially after corrections have been applied. For example, from this experiment and others[1] the variance was determined to be ≤ 0.01. Moreover, these errors tend to influence amplitudes in $\chi(k)$ more than frequencies, and frequencies are more important for deriving structural information. Typically, uncertainties of ca $\pm$ 0.01Å are introduced into near-neighbor distances by these "physical" errors. More troublesome, in part because they are in principle unnecessary, are errors arising from inadequacies in the non-structural factors such as the inner potential and scattering phase shifts used in the MSSW calculation to fit the data. These problems are also present in EXAFS, surface EXAFS, and LEED studies as well. They become important when accuracies in the 0.01-0.02Å range are sought. Further improvement in understanding these issues is on our agenda for future development of the ARPEFS method. All things considered, we believe that the accuracy of our structural analysis for c(2x2)S/Fe(001) is typically $\pm$ 0.02Å in the parameters to which our $\chi(k)$ curves are sensitive. There is also an ameliorating feature concerning these non-structural errors. Namely, relative distances, for example to substrate planes, are probably more accurate than would be implied by adding the errors even in quadrature, because of systematic cancellation of errors.

Analysis of ARPEFS data is sensitive to lattice expansion or contraction and to corrugation of the substrate second layer, if present. For example, Bahr et al.[23] found 0.13Å second-layer corrugation in p(2x2)S/Cu(001), while Robey at al.[24] found 9% first-second layer contraction and 8% second-third layer expansion in (2x2)S/Ge(111). In the present case of c(2x2)S/Fe(001), we found a 0.03Å first-second layer contraction, a 0.03Å second-third layer expansion, and no evidence for second-layer corrugation. The two different S-Fe_{II} distances were varied to test for second-layer buckling and none was found within the assigned error limits.

A discussion of adsorbate-substrate bonding in c(2x2)S/Fe(001) should consider both chemical and steric issues. To provide a context and establish a base for the discussion of systematic trends, we set out in Table II the values of a number of relevant parameters for sulfur adsorbed on Cr, Fe, Cu, Ni, and Mo, taken from references cited above and others.[25-31]

In examining these values we have noticed a systematic relation between "channel size" in the first layer and S-M_2 distance, where M_2 is the second-layer metal atom directly below sulfur. The channel size is defined by imagining cutting the adsorbate atom and two diagonally opposite first-layer atoms with a plane normal to the surface. Using the Pauling bond radii R(1) of the substrate atom, we can compute the open space along the diagonal, which we take to be the channel diameter d. The order of d sizes is

$$\text{Ni(011)} > \text{Mo(001)} > \text{Fe(001)} \sim \text{Cr(001)} > \text{Ni(001)} > \text{Cu(001)}.$$

Here the reconstructed Cu(001) value[23] has been used: significant lateral reconstruction was allowed by the p(2x2) surface symmetry in this case alone. Now this order is almost opposite to that of the S-M_2 distance, R(S-M_2):

$$Ni(011) < Cr(001) < Fe(001) < Mo(001) < Cu(001) < Ni(001).$$

A more meaningful comparison is that of the trend in d with the difference, Δ, between R(S-M_2) and the sum of the Pauling bond radii, R(S) + R(M), which corrects for differences in R(M). This order is:

$$Ni(011) < Mo(001) < Cr(001) < Fe(001) < Cu(001) < Ni(001).$$

The M-S-M bond angle gives a similar order:

$$Ni(011) > Mo(001) > Fe(001) > Cr(001) > Ni(001) > Cu(001).$$

Both orders correlate better with the channel size d. For convenience these parameters are set out separately in Table III. Because quantitative comparisons are better illustrated graphically, we also plot in Fig. 8 the values of both Δ and $\angle$(M-S-M) against d. The geometry is shown in Fig. 9.

In the conventional chemical language of forming covalent bonds through overlap of directed atomic orbitals, we can proceed as follows.[4,6,7] Sulfur $3p_x$ and $3p_y$ orbitals can form π bonds with d_{xz} and d_{yz} orbitals on the four nearest-neighbor first-layer substrate atoms

around the fourfold hollow site. If we imagine the sulfur atom moving down the surface normal into the hollow site, the energy will be lowered by this p-π bonding to first-layer atoms and by σ bonding to the second-layer atom directly below, if it is accessible. The latter will only be important for cases in which the fourfold site is sufficiently open to provide a channel large enough to admit the sulfur atom at least partially. For a relatively closely packed surface layer, steric (repulsive) forces will prevent sulfur from approaching closely enough to form a significant bond to the second-layer atom.

This bonding model is consistent with the experimental results depicted in Fig. 10. The M-S-M bond angle takes on several values between 102° and 138°, consistent with p-π to $d_{xz,yz}$ bonding (but not, for example, with strongly directional σ hydrid bonding on sulfur, at least not with the same hybridization in all six cases). The M-S-M bond angle increases with channel size, as the sulfur site moves down into the channel. Finally, sulfur penetrates the channel to various depths with increasing channel size, until in c(2x2)S/Ni(001) the S-M_2 distance reaches the Pauling bond radii value.

While the above simplified bonding model supports the experimental results, the converse is unfortunately only weakly true. It is correct, as noted above, that certain imaginable competitive models of strongly directional bonding are ruled out, and the results show unambiguously that S and M_2 interact attractively rather than repulsively. However, other models can also fit the data. For example, all the results in Table III and Fig. 8 could be derived by assuming the atoms to be fairly hard spheres, with negative charge on the sulfur and positive charges on

the first and second-layer metal atoms. To go further in differentiating among empirical bonding models we would have to consider (and explain) the observed lattice relaxation effects. After inspecting the data we became convinced that explanation of the observed relaxation effects with a simple valence-bond model would require more arbitrary parameters than we have structural parameters. We are fairly convinced that the M_1-M_2 distance in both c(2x2)S/Fe(001) and c(2x2)S/Cr(001) is shortened because sulfur fits down far enough in the hollow site to attract the M_2 atom up by a small amount. In c(2x2)S/Ni(011), on the other hand, the sulfur atom can bond directly to Ni_2 ($R(S\text{-}Ni_2)$=2.18Å) in the very open site, then shorten and strengthen its bonds to the four first-layer Ni atoms by pressing Ni_2 down, thereby effecting the observed Ni_1-Ni_2 expansion. Beyond these three cases, however, we hesitate to interpret the observed relaxations without a better theoretical model.

In this context we quote the result of a SCF Xα SW calculation with a nonempirical scheme for choosing overlapping sphere radii.[2] A 9-atom Fe cluster was used, in the observed experimental geometry, and the S-Fe_1 distance was allowed to vary by moving S along the normal. The total energies for six geometries are listed in Table IV and the variation of total energy with $R(S\text{-}Fe_1)$ is depicted in Fig. 10. Remarkably, the energy minimum lies at the experimental geometry. Furthermore, placing the Fe atoms in positions corresponding to the bulk geometry increases the total energy substantially. Thus apparently the SCF Xα SW model calculation is capable of accounting for the local lattice relaxation. If this finding is confirmed for other simple

adsorbate systems, the SCF Xα SW model may prove very useful. In trying to understand this unexpectedly good result, we note that the model is not being asked to find an absolute energy minimum or an accurate minimum energy. Rather it is being asked to respond to the variation of one parameter, $R(S\text{-}Fe_1)$, and to a change in $R(Fe_1\text{-}Fe_2)$. Further study is clearly warranted.

ACKNOWLEDGEMENTS

This work was supported by the Director, Office of Energy Research, Office of Basic Energy Sciences, Chemical Sciences Division of the U.S. Department of Energy under Contract No. DE-AC03-76SF00098. It was performed at the Stanford Synchrotron Radiation Laboratory, which is supported by the Department of Energy's Office of Basic Energy Sciences.

References

1. L.J. Terminello, X.S. Zhang, Z.Q. Huang, S. Kim, A.E. Schach von Wittenau, and D.A. Shirley, (submitted to Phys. Rev. B.).
2. X.S. Zhang, L.J. Terminello, A.E. Schach von Wittenau, S. Kim, Z.Q. Huang, Z.Z. Yang, D.A. Shirley, F.M. Tao, and Y.K. Pan (in preparation).
3. K.O. Legg, F. Jona, D.W. Jepsen, and P.M. Marcus, Surf. Sci. 66, 25 (1977).
4. R.A. DiDio and E.W. Plummer, J. Vac. Sci. Technol. A2, 983 (1984).
5. G. Panzner and B. Egert, Surf. Sci. 144, 651 (1984).
6. G.W. Fernando and J.W. Wilkins, Phys. Rev. B 33, 3709 (1986).
7. G.W. Fernando and J.W. Wilkins, Phys. Rev. B 35, 2995 (1987).
8. J.J. Barton, S.W. Robey, C.C. Bahr, and D.A. Shirley, 1st Intl. Conf. on the Structure of Surfaces, Berkeley, CA, Springer Series in Surface Science 2nd ed., edited by M.A. van Hove and S.Y. Tong (1985).
9. J.J. Barton and D.A. Shirley, Phys. Rev. A 32, 1019 (1985).
10. J.J. Barton, S.W. Robey, and D.A. Shirley, Phys. Rev. B 34, 778 (1986).
11. Z. Hussain, E. Umbach, D.A. Shirley, J. Stohr, and J. Feldhaus, Nucl. Instrum. Methods 195, 115 (1982).
12. S.D. Kevan, Ph.D. thesis, University of California, Berkeley, 1980 Lawrence Berkeley Laboratory Report LBL-11017 (unpublished).
13. P.B.V. Narayan, J.W. Anderegg, and C.W. Chen, J. Elect. Spectros. and Rel. Phen 27, 233 (1982).

14. M.R. Shanabarger, Proceedings of the 8th International Vacuum Congress, Cannes, Vide, Couches Mincos (VCMIDS), (Suppl., Proc. Int. Conf. Solid Surface, 4th, V1), 1980, vol. 201, pp. 494-97.

15. J.J. Barton, Ph.D. thesis, University of California, Berkeley, 1985 Lawrence Berkeley Laboratory Report LBL-19215 (unpublished).

16. J.J. Barton, C.C. Bahr, S.W. Robey, Z. Hussain, E. Umbach, and D.A. Shirley, Phys. Rev. B 34, 3807 (1986).

17. P.A. Lee, P.H. Citrin, P. Eisenberger, and B.M. Kincaid, Rev. Mod. Phys. 53, 769 (1981).

18. See Footnote 11 and Fig. 5 in Reference 3.

19. J.B. Pendry, Low Energy Electron Diffraction, (Academic Press, London, 1974).

20. V.L. Moruzzi, J.F. Janak, and A.R. Williams, Calculated Electronic Properties of Metals, (Pergamon Press, New York, 1978).

21. S.W. Robey, J.J. Barton, C.C. Bahr, G. Liu, and D.A. Shirley, Phys. Rev. B 35, 1108 (1987).

22. R.E. Allen, G.P. Alldredge, and F.W. de Wette, J. Chem. Phys. 54, 2605 (1971).

23. C.C. Bahr, J.J. Barton, Z. Hussain, S.W. Robey, J.G. Tobin, and D.A. Shirley, Phys. Rev. B 35, 3773 (1987).

24. S.W. Robey, C.C. Bahr, Z. Hussain, J.J. Barton, K.T. Leung, Ji-ren Lou, A.E. Schach von Wittenau, and D.A. Shirley, Phys. Rev. B 35, 5657 (1987).

25. L. Pauling, The Nature of the Chemical Bond, (Cornell Univ. Press, Ithaca, NY, 1960).

26. C.C. Bahr, S.W. Robey, Z. Hussain, K. T. Leung, Ji-ren Lou, L.J. Terminello, A.E. Schach von Wittenau, and D.A. Shirley, (unpublished).

27. K.A.R. Mitchell, Surf. Sci. 100, 225 (1980).

28. D.L. Adams and U. Landman, Phys. Rev. B 15, 3775 (1977).

29. J.E. Demuth, P.M. Marcus, and D.W. Jepsen, Phys. Rev. B 11, 1460 (1975).

30. J.B. Pendry, J. Phys. C 4, 2514 (1971).

31. A. Ignatiev, F. Jona, and H.D. Shih, D.W. Jepsen, and P.M. Marcus, Phys. Rev. B 11, 4787 (1975).

Table I. Derived structural parameters for c(2x2)S/Fe(001). Errors in last place are shown in parentheses.

Source	Interlayer Spacing (Å)			Angle	Ref.
	S-Fe_I	Fe_I-Fe_{II}	Fe_{II}-Fe_{III}	Fe_I-S-Fe_I	
LEED	1.09(5)	[1.43]			3
	[1.05]				18
ARPEFS					
[001] data	1.10(2)	1.40(2)	1.45(3)		this work
[011] data	1.09(2)	1.40(3)	1.46(3)		this work
Adopted Value	1.10(2)	1.40(2)	1.46(3)	122.9(9)°	this work

Table 2. The structural parameters (in Å) of sulfur adsorbed on metals. R(1) are the Pauling bond radii. D(1) is a single bond length taken as the sum of the single bond radii of sulfur (1.04 Å) and R(1).

			$S\text{-}X_I$		$S\text{-}X_{II}$	$X_I\text{-}X_{II}$						
			Bond	inter	Bond	After	Clean Surf		Δ, (S ads. -		Lattice	
Substrate	R(1)[a]	D(1)	length	layer	length	S. adsorp.	surf.	relax.	clean), x %	Bulk	constant	Refs.[b]
Ni(011)	1.154	2.19	2.31	0.82	2.18	1.36	1.175	-5%	+15.7%	1.24	3.52	21,29
Cr(001)	1.186	2.23	2.35	1.17	2.49	1.32	?	?	-8.3%[c]	1.44	2.88	1
Fe(001)	1.17	2.21	2.30	1.10	2.50	1.40	1.41	-1.4%	(~ 0.7%)	1.43	2.86	d, 27
Mo(001)	1.296	2.34	2.41	0.92	2.54	1.62	1.39	-11.5%	+16.6%	1.57	3.15	26,31
Cu(001)	1.176	2.21	2.26	1.42	3.04	1.62	1.80	0	-10%	1.81	3.61	23,28
Ni(001)	1.154	2.19	2.19	1.30	3.14	1.84	1.78	+1%	+3.4%	1.76	3.52	16,29

[a]From Ref. 25.

[b]The first citation is to the adsorbate system, and the second to the clean surface in each case.

[c]Compared to the bulk distance.

[d]This work.

Table 3. Size Parameters for Sulfur Adsorbate Systems

Surface	Channel Size d (Å)	S-M_2(Å)	R_S+R_M, (Å)	Δ, (Å)	∠(M-S-M)
Ni(011)	2.00	2.18	2.19	(-0.01)	138°
Mo(001)	1.86	2.54	2.41	0.13	135°
Fe(001)	1.704	2.50	2.21	0.29	123°
Cr(001)	1.70	2.49	2.23	0.26	120°
Ni(001)	1.21	3.14	2.19	0.95	107°
Cu(001)	1.16	3.04	2.21	0.83	102°

Table 4. The list of total energies of c(2x2)S/Fe via the variation of the interlayer distance S-Fe_I derived from SCF Xα SW calculations on a 9-atom Fe cluster simulating the S/Fe(001) local geometry. The last row is the structure with same S-Fe_I but bulk frame of iron (Fe_I-Fe_{II} = 1.43 ± 0.02 Å). The difference of total energies is relative to the total energy of the experimental geometry (from reference 2).

Interlayer S-Fe_I	Total Energy (Rydbergs)	Δ Total Energy (rel. to 1.09 Å)
1.14 Å	-23518.134	2.40 eV
1.115 Å	-23518.247	0.855 eV
1.09 Å	-23518.310	0
1.065 Å	-23518.235	1.02 eV
1.04 Å	-23518.115	2.65 eV
1.09 Å (used Fe bulk frame Fe_I-Fe_{II} = 1.43 Å)	-23518.029	3.82 eV

Figure Captions

Figure 1. A view of the c(2x2)S/Fe(001) surface, showing the two emission directions, [001] and [011]. Dark atoms represent sulfur, light atoms are the bulk iron.

Figure 2. χ(k) curves are shown for the normal ([001]) and off-normal ([011]) emission directions. Each curve is the fractional modulation of the S(1s) intensity as a function of photoelectron wavevector for the indicated direction.

Figure 3. Fourier transforms of the χ(k) data given in Fig. 2. Each numbered peak in the Fourier spectrum can be qualitatively assigned to scattering events from particular atoms (see Fig. 4) near the photoemitter.

Figure 4. The side view of the c(2x2)S/Fe(001) system illustrates the scattering atoms (numbered substrate atoms) that dominate the Fourier power spectra of Fig. 3. Scattering path-length differences for each numbered scatterer are referenced to the photoemitter(s).

Figure 5. A comparison of MSSW calculation is shown for three non-optimized geometries (atop, bridge, and fourfold hollow sites) with the experimental data for the [001] direction.

Figure 6. MSSW calculations and experimental curve for the [011] direction data.

Figure 7. The best fit MSSW curve (dashed line) is compared to the experimental data (solid line). The geometry used to generate the simulated curves is listed in Table I.

Figure 8. The sulfur adsorption angle ($\angle$M-S-M) and the adsorbate-to-second layer distance (Δ) are presented as functions of the

channel width (d). These values are defined in the text and illustrated in Fig. 9.

Figure 9. Illustrated is the sulfur adsorption site in a plane perpendicular to the surface and diagonally through the fourfold hollow site (a plane parallel to [110] and through the adsorbate). Δ is the open space defined by the Pauling bond radii between the sulfur and second layer metal atom. d is the open space along the fourfold diagonal. ∠M-S-M is the angle made by the two first layer metal atoms and sulfur.

Figure 10. The SCF Xα total energy is plotted relative to the minimum energy calculated (Δ total energy from table IV) and as a function of the sulfur to first layer iron distance. The data points calculated follow a parabolic fit (solid line).

c(2X2)S/Fe(001)

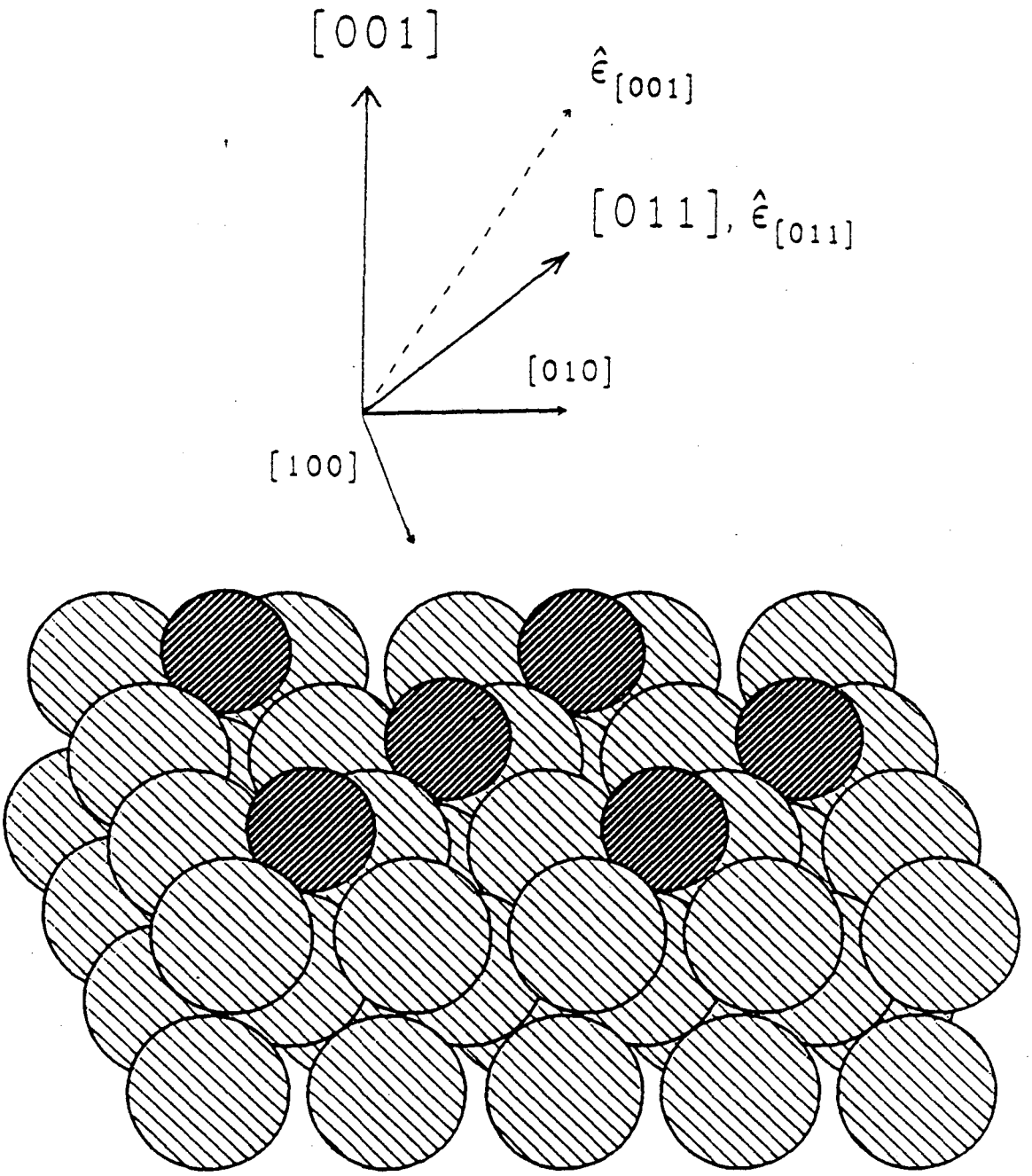

XBL 884-1319

Figure 1

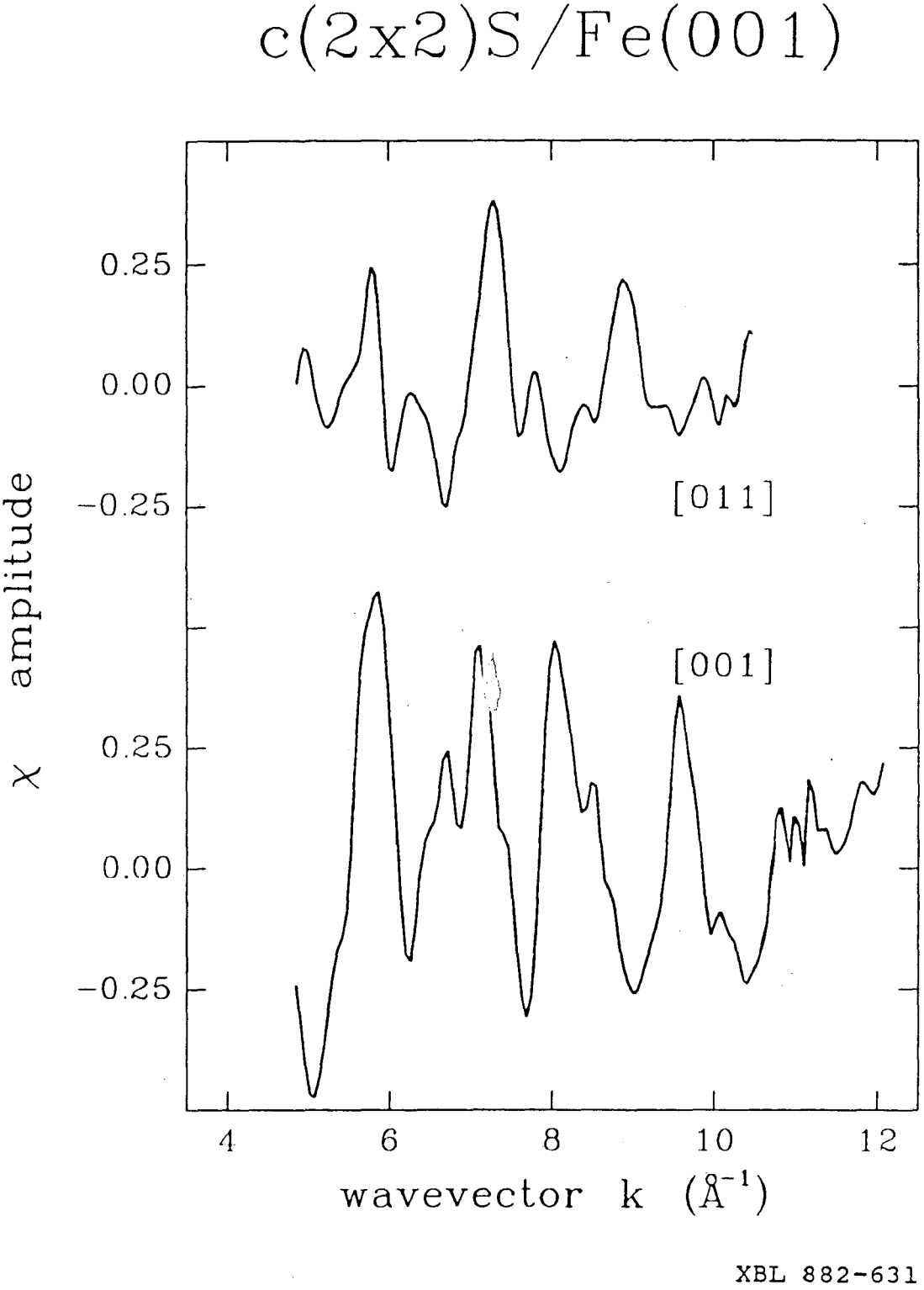
c(2x2)S/Fe(001)
0.25
0.00
−0.25
[011]
[001]
0.25
0.00
−0.25
χ amplitude
4
6
8
10
12
wavevector k (Å⁻¹)
XBL 882-631

Figure 2

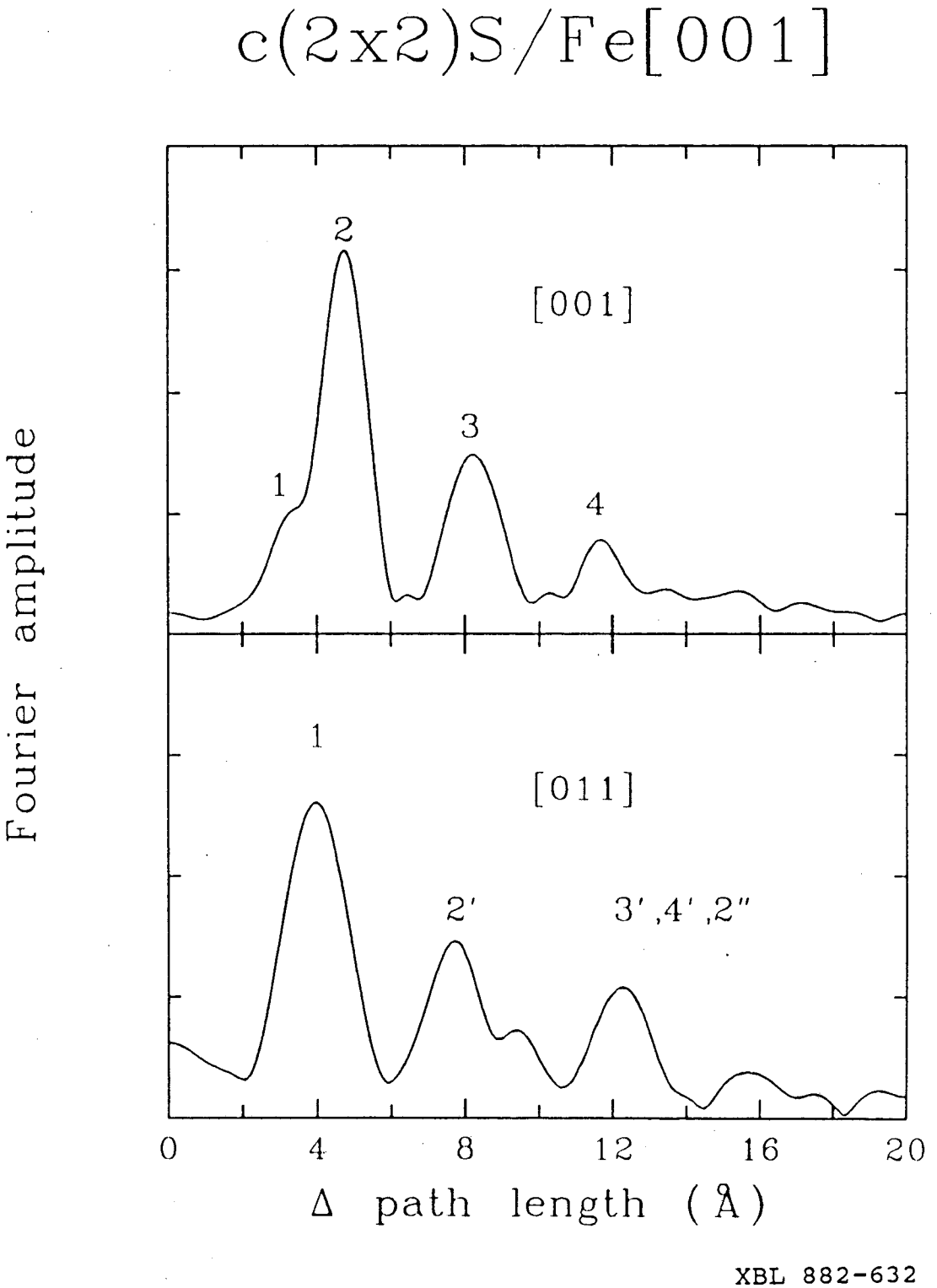
c(2x2)S/Fe[001]
Fourier amplitude
2
[001]
3
1
4
1
[011]
2'
3',4',2"
0
4
8
12
16
20
Δ path length (Å)
XBL 882-632

Figure 3

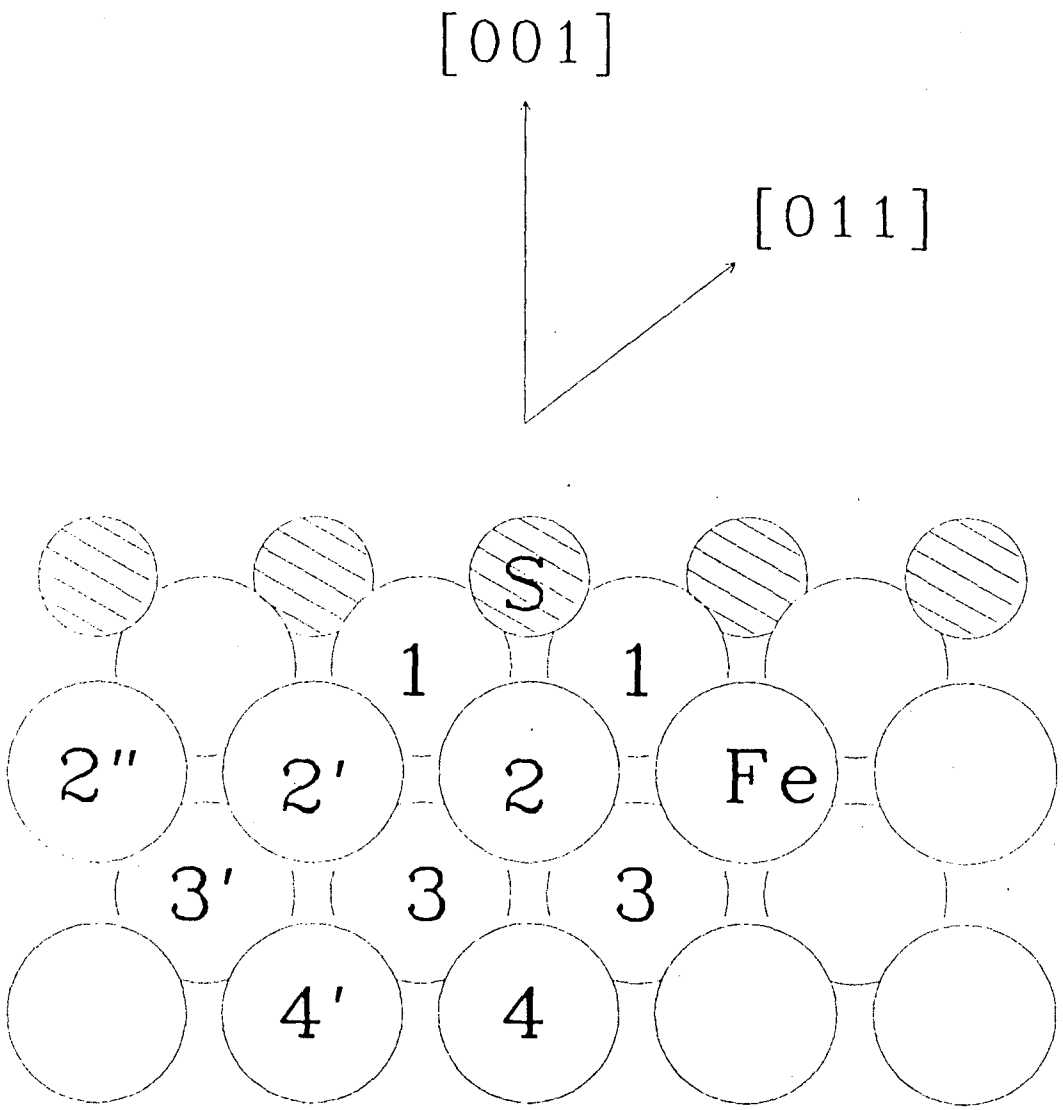

XBL 882-630

Figure 4

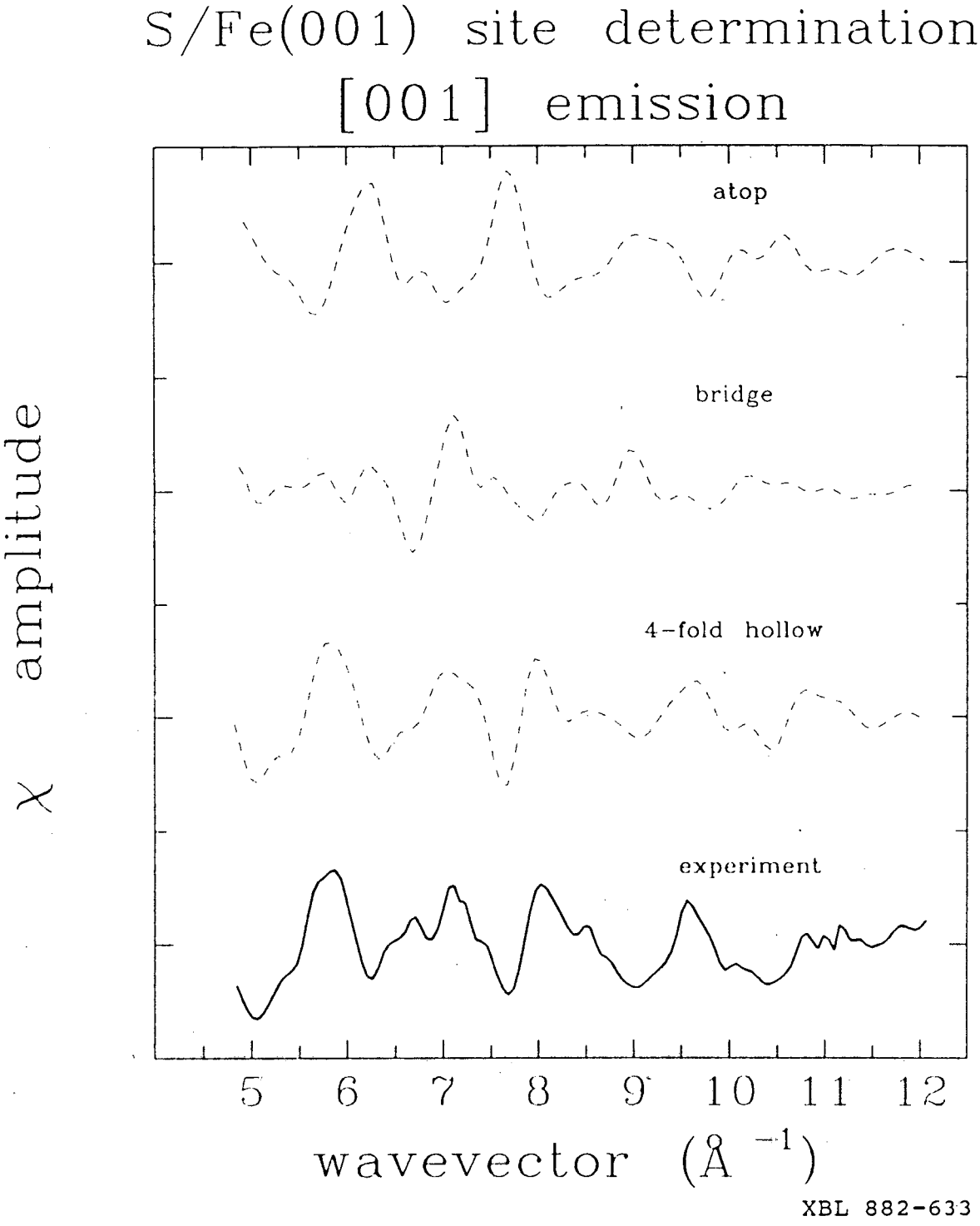
S/Fe(001) site determination
[001] emission
atop
bridge
4-fold hollow
experiment
χ amplitude
5
6
7
8
9
10
11
12
wavevector (Å⁻¹)
XBL 882-633

Figure 5

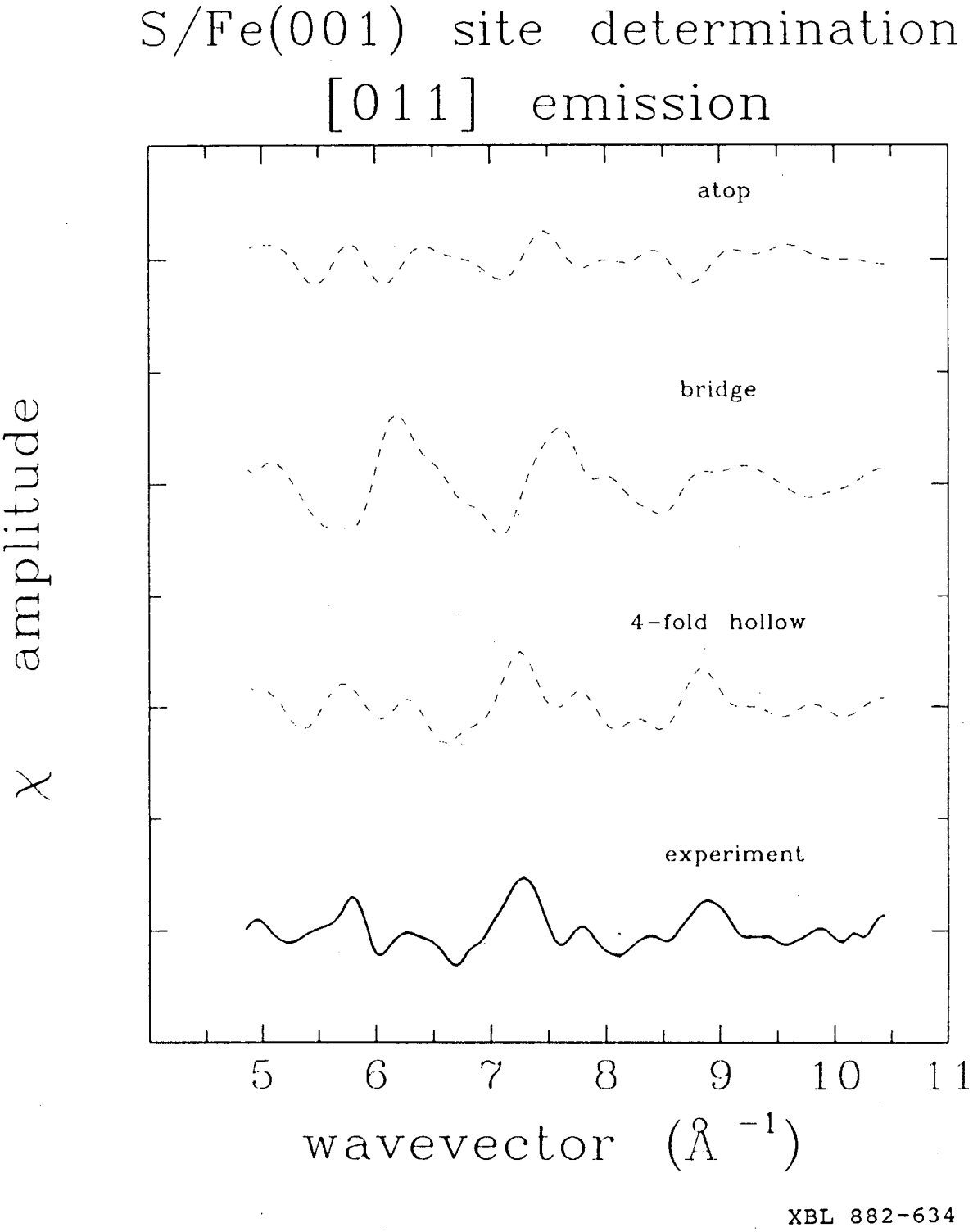
S/Fe(001) site determination
[011] emission
atop
bridge
4-fold hollow
experiment
χ amplitude
5
6
7
8
9
10
11
wavevector (Å^{-1})
XBL 882-634

Figure 6

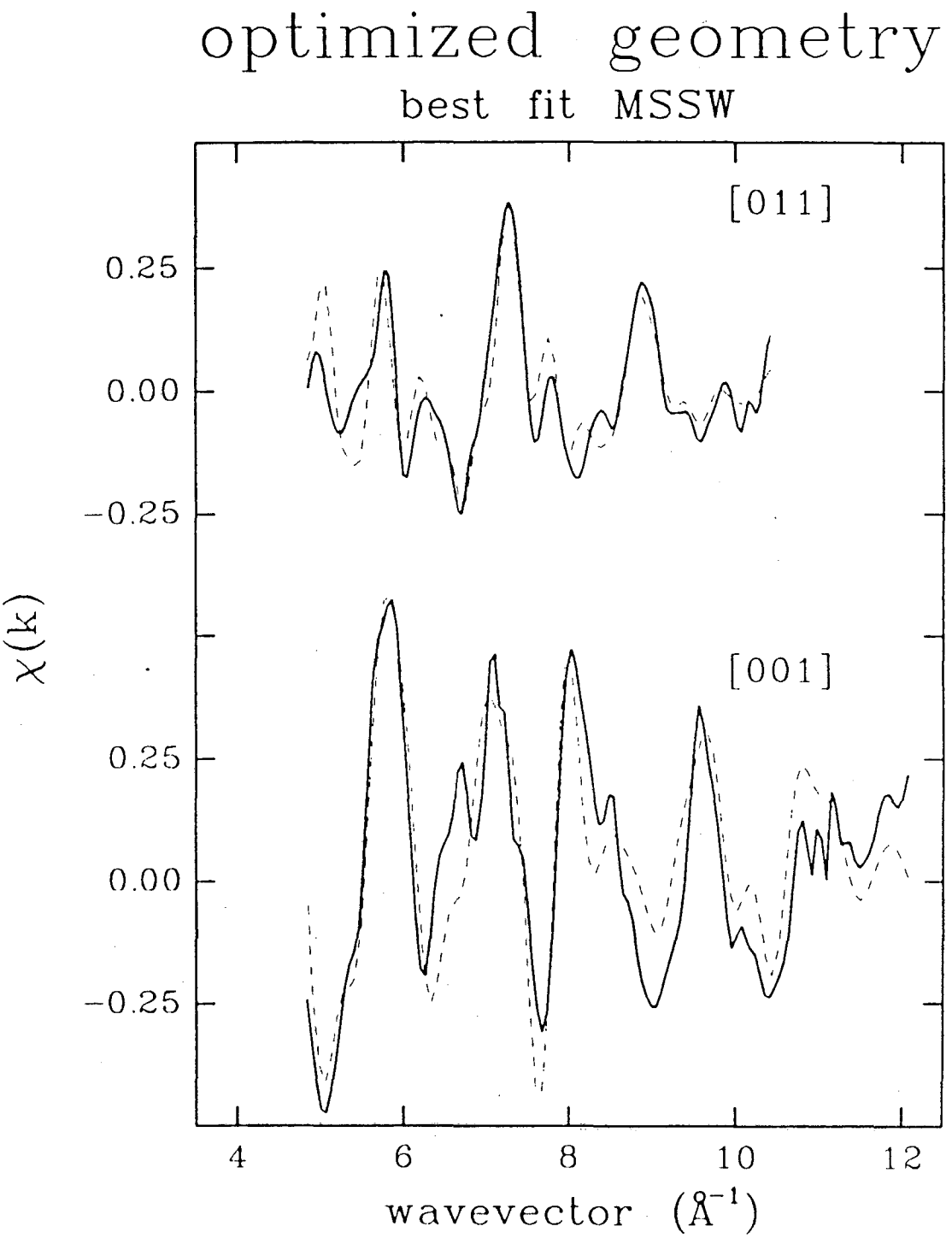

XBL 882-635

Figure 7

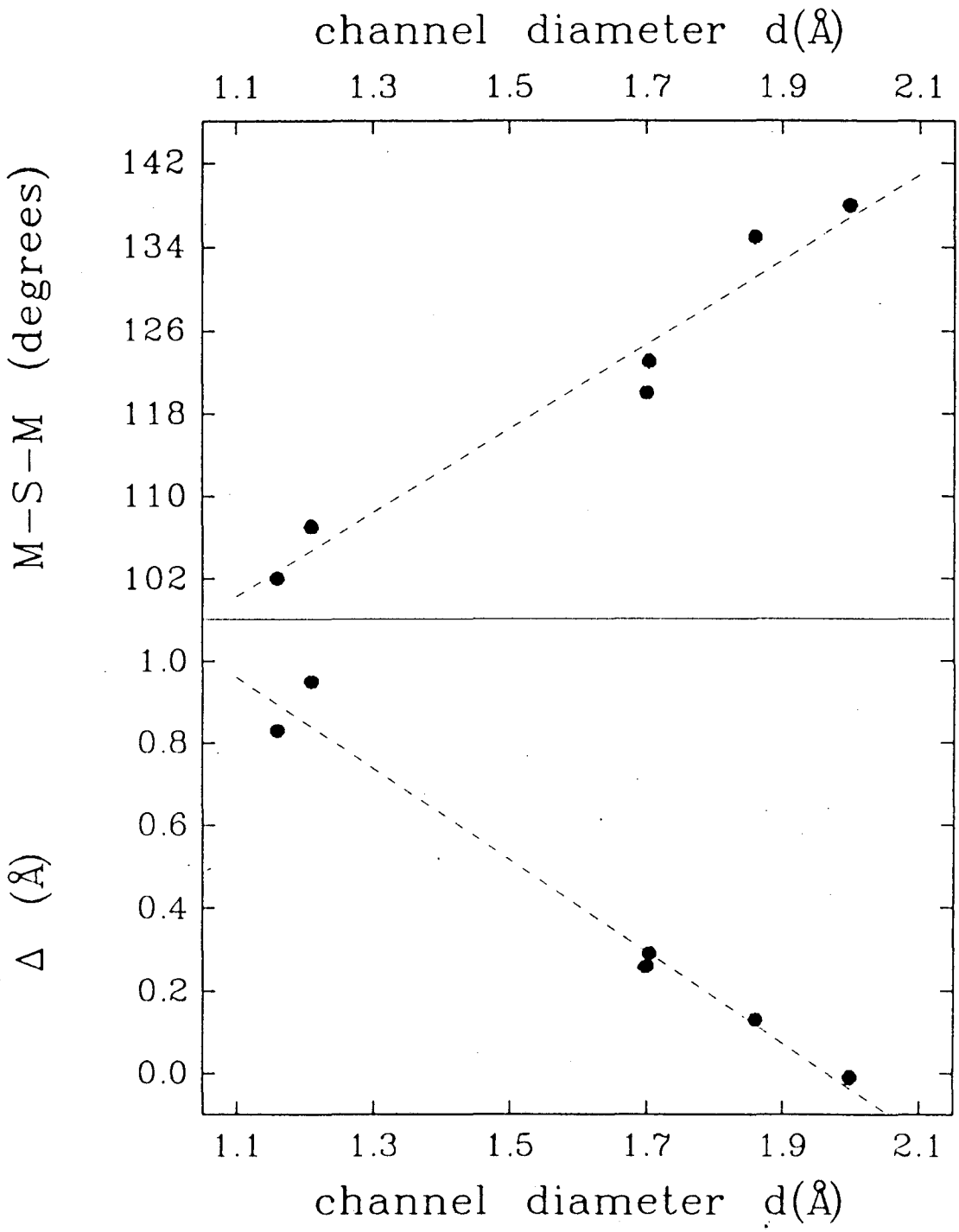

XBL 882-638

Figure 8

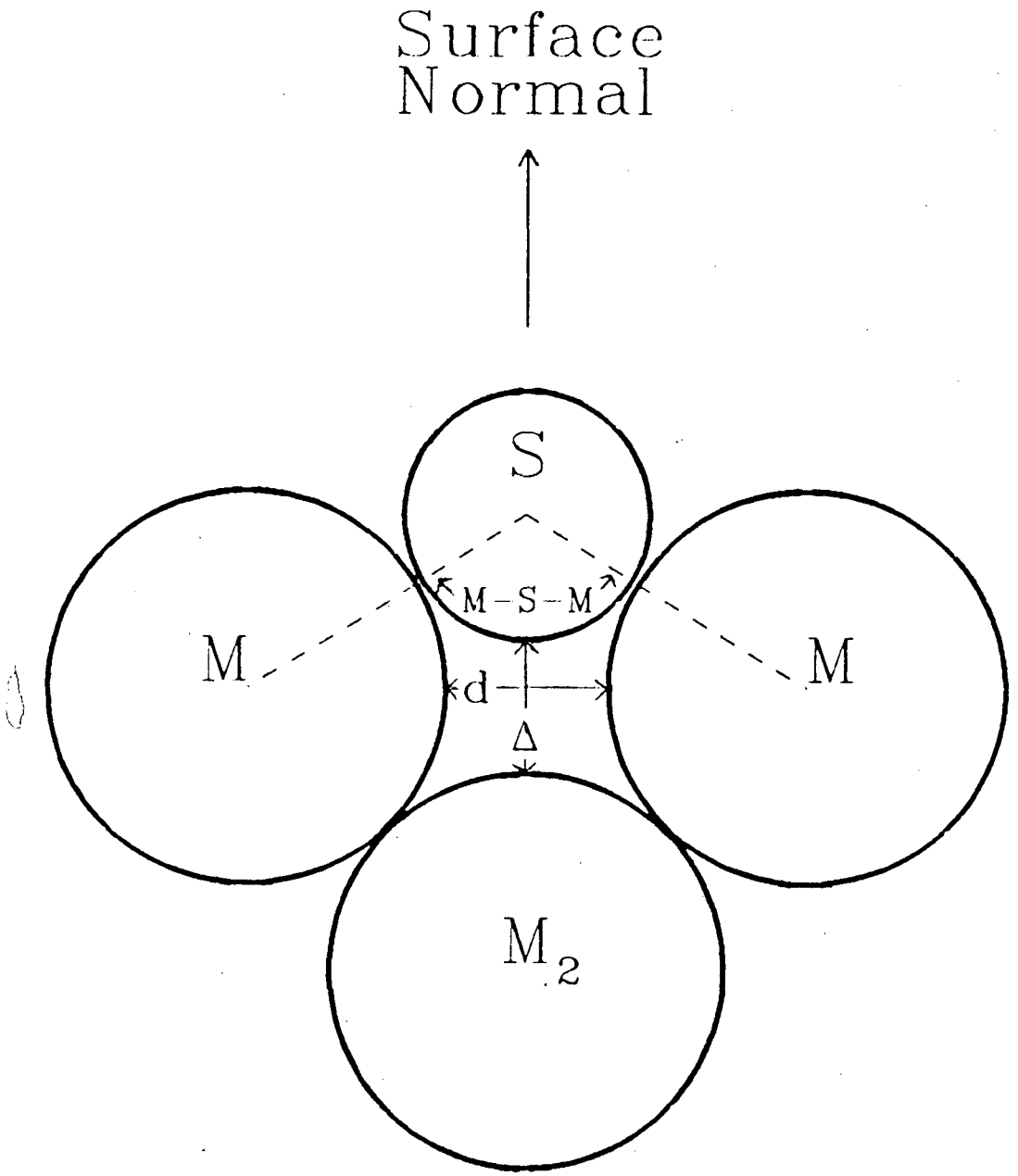

XBL 882-636

Figure 9

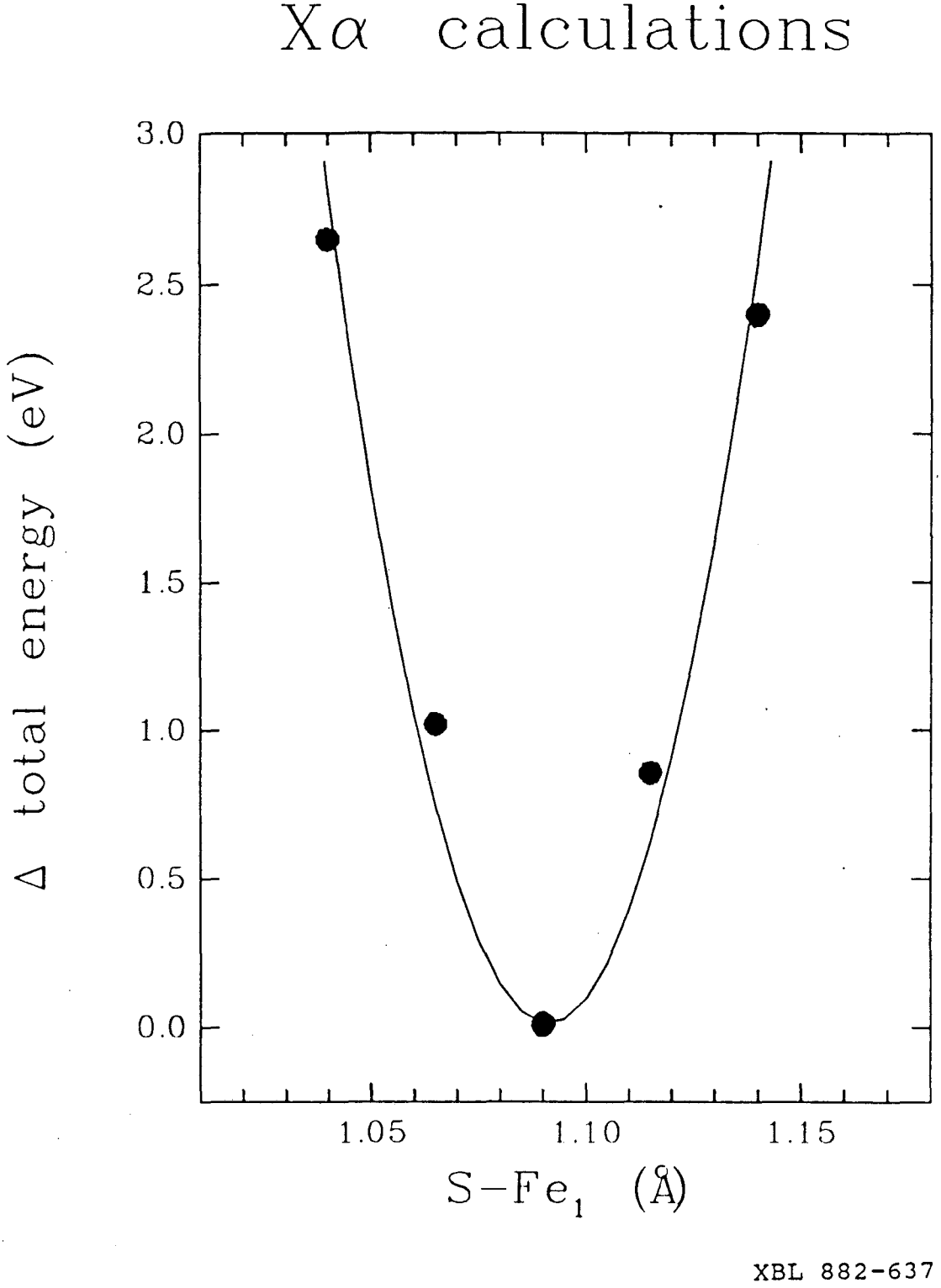
Xα calculations
3.0
2.5
2.0
1.5
1.0
0.5
0.0
Δ total energy (eV)
1.05
1.10
1.15
S−Fe1 (Å)
XBL 882-637

Figure 10

LAWRENCE BERKELEY LABORATORY
TECHNICAL INFORMATION DEPARTMENT
UNIVERSITY OF CALIFORNIA
BERKELEY, CALIFORNIA 94720